Available online at www.sciencedirect.com
ScienceDirect
Trans. Nonferrous Met. Soc. China 31(2021) 734−743
Transactions of Nonferrous Metals Society of China
www.tnmsc.cn

Effects of annealing at 800 and 1000 °C on phase precipitates and hardness of $Al_7Cr_{20}Fe_xNi_{73-x}$ alloys

Chang-jun WU[1,2], Chen ZHOU[1], Jiao-feng ZENG[1], Ya LIU[1,2], Hao TU[1,2], Xu-ping SU[1,2]

1. Jiangsu Key Laboratory of Materials Surface Science and Technology, School of Materials Science and Engineering, Changzhou University, Changzhou 213164, China;
2. Jiangsu Collaborative Innovation Center of Photovoltaic Science and Engineering, Changzhou University, Changzhou 213164, China

Received 9 April 2020; accepted 15 January 2021

Abstract: The effects of Fe content on the microstructure, phase constituents and microhardness of the as-cast, 800 °C- or 1000 °C-annealed $Al_7Cr_{20}Fe_xNi_{73-x}$ (x=13−66) alloys were investigated. Not all these alloys are composed of the single FCC phase. The BCC and $B2$ phases are found. It is confirmed that the BCC phase in the $Al_7Cr_{20}Fe_{66}Ni_7$ alloy is transformed from the FCC phase at about 900 °C during cooling. While in the 800 °C-annealed $Al_7Cr_{20}Fe_{60}Ni_{13}$ alloy, the FCC phase is stable and the hardness decreases. After annealing at 1000 °C, for the precipitation of the $B2$ particles, the Al content in the FCC phase decreases, which results in decreasing of the alloy hardness. Moreover, after annealing at 800 °C, a small amount of Al-rich $B2$ particles precipitate at the phase boundary and some nanocrystal BCC phase precipitates in the FCC matrix, which increases the hardness of the $Al_7Cr_{20}Fe_xNi_{73-x}$ (x=41−49) alloys. These results will help to the composition design and processing design of the Al−Cr−Fe−Ni based high-entropy alloys.
Key words: high-entropy alloy; Al−Cr−Fe−Ni; phase constituent; microhardness; heat treatment

1 Introduction

High-entropy alloys (HEAs) are presently of great research interest in materials science and engineering. According to the initial definition, HEAs are super solid solution alloys with more principal elements than conventional alloys [1]. Their microstructures and properties have attracted much attention. At present, an increasing number of works about HEAs, including novel microstructures and excellent properties, have been reported. Amongst them, AlCrFeNi-based HEAs have been widely investigated, such as AlCoCrFeNi [2−6], AlCrFeNiMo [7], AlCrFeNiTi [8], AlCrFeMnNi [9], AlCoCrCuFeNi [10−14], AlCrMnFeCoNi [15], and AlCoCrFeMoNi [16−18]. The matrices of these alloys are FCC and/or BCC phases, which vary with the alloy composition and are significantly affected by the atomic-size difference (ΔR) and valence electron concentration (VEC) [4,19,20]. Some alloys have unexpected properties. For example, after annealing at 800−1200 °C, the $AlCoCrFeNi_{2.1}$ alloy [5] has a good tensile ductility over 10% as well as a high tensile strength larger than 1000 MPa. The $AlCrFeNiMo_{0.2}$ alloy [7] has the highest fracture strength of 3222 MPa and a plastic strain of 0.287. Of course, the properties of the alloys can also be modified by adjusting their composition, cooling rate and thermal–mechanical processing. CHEN et al [21] pointed out that the excellent strain-hardening ability in the $Al_{0.1}CoCrFeNi$ alloy was attributed to the microband-induced plasticity during tensile loading.

Corresponding author: Xu-ping SU; Tel: +86-519-86330016 ; E-mail: sxping@cczu.edu.cn
DOI: 10.1016/S1003-6326(21)65534-6

As a subsystem, many Al−Cr−Fe−Ni alloys have been investigated. It is well known that Al is a BCC-stabilizing element in the Al−Cr−Fe−Ni based HEAs. Only the FCC phase exists in the $Al_7Cr_{20}Fe_{20}Ni_{53}$ alloy [22]. When Al content reaches above 8 at.%, the ordered BCC phase (*B*2) will form [22−24]. With an increase of the Al content, the volume fraction of the *B*2 phase increases; the alloy exhibits increased strength and reduced ductility [15,23,24]. Generally, when the Al content is above 24 at.%, the Al−Cr−Fe−Ni alloys consist of BCC and/or *B*2 phases, such as $Al_xCrFeNi$ (x=0.9−1.3) [25−27], $Al_{36}Fe_{20}Cr_{20}Ni_{24}$ [22], $Al_xCrFe_{1.5}Ni_{0.5}$ [28], and $AlCrFe_2Ni_2$ [29]. The Al−Cr−Fe−Ni system is also of interest for the existence of two types of eutectic point, namely, the FCC+*B*2 eutectic in $CrFeNi_{2.2}Al_{0.8}$ alloy [30] and the BCC+*B*2 eutectic in $Al_xCrFeNi$ alloys [26,27]. Both of them show good mechanical properties. Moreover, YAO et al [31] found that the phase constituents varied with the Ni content in the $Al_{0.8}CrFe_2Ni_x$ alloys.

The FCC matrix alloys always have good formability. As indicated above, the BCC or *B*2 phase did not exist in $Al_7Cr_{20}Fe_{20}Ni_{53}$ alloy [25], but it was observed in the Al−Cr−Fe−Ni alloys when the Al content is above 8 at.% [24,25,28]. That is to say, 7 at.% Al is near the boundary of the FCC phase region. Moreover, the phase constituents, microstructures and mechanical properties are greatly changed after annealing [32], and even can be changed by the cooling rate in powder prepared alloys [6]. However, it was found that thermodynamic calculations based on the available thermodynamic database failed to predict the stable phase in these Al−Cr−Fe−Ni alloys. To understand the effects of Fe and Ni contents on the phase constituent of the Al−Cr−Fe−Ni alloys, in the present work, Al and Cr contents were fixed at 7 and 20 at.%, respectively. The microstructure, phase transformation and micro-hardness of the as-cast and long duration vacuum-annealed alloys were studied. These results will help to design the composition and process of the Al−Cr−Fe−Ni based high-entropy alloys.

2 Experimental

Eight $Al_7Cr_{20}Fe_xNi_{73-x}$ alloys, with the Al and Cr content fixed at 7 at.% and 20 at.%, respectively, were designed to study the effects of the Fe content and annealing on the phase constituents and microhardness of the alloys in the as-cast and vacuum-annealed states. The raw materials of Al, Cr, Fe and Ni blocks with a purity higher than 99.95% were used. The total mass of each alloy was designed to be 10 g. All ingots were manufactured by vacuum arc-melting and casting under a Ti-gettered argon atmosphere inside a water-cooled copper crucible. They were re-melted at least four times to improve their chemical homogeneity. Each alloy was divided into three parts. One part was studied in the as-cast state and the others were sealed in evacuated quartz tubes and then annealed at 1000 or 800 °C for 30 d, respectively. The samples were quenched in cold water at the end of treatment. In order to distinguish the alloys in different states, the as-cast alloys are denoted as "A", and the 1000 °C and 800 °C annealed alloys are marked as "A′" and "A″", respectively.

The microstructures of the samples were examined by JSM−6510 scanning electron microscopy (SEM) and the chemical compositions were investigated by Oxford INCA energy dispersive spectroscopy (EDS). The structure of the samples was characterized by X-ray diffraction (XRD) using a D/max 2500 PC X-ray diffractometer with Cu K_α radiation and a 2θ step size of 0.02°. The microstructure of the selected samples was also characterized by an FEI Talos F200X TEM. Microhardness was measured using a HXD−1000TMC/LC Vickers hardness tester under a load of 2.94 N and stayed for 15 s. The average value of five tests was taken as the hardness of the alloy.

3 Results and discussion

3.1 As-cast $Al_7Cr_{20}Fe_xNi_{73-x}$ alloys

The XRD patterns and back-scattered electron (BSE) images of the as-cast $Al_7Cr_{20}Fe_xNi_{73-x}$ alloys prepared by arc-melting are shown in Fig. 1 and Fig. 2, respectively. The chemical composition of the alloys and the phases detected by SEM−EDS are listed in Table 1. As can be seen in Fig. 1, with fixed 7 at.% Al and 20 at.% Cr, the phase constituents of the as-cast $Al_7Cr_{20}Fe_xNi_{73-x}$ alloys gradually change from FCC-type to BCC-type phase with an increase of the Fe content.

As there is no evidence to support that the FCC-type phase is an ordered one, it is believed

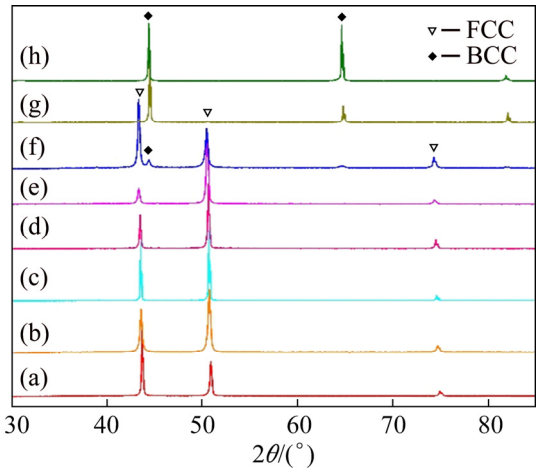

Fig. 1 XRD patterns of as-cast $Al_7Cr_{20}Fe_xNi_{73-x}$ alloys: (a) Alloy A1 (x=13); (b) Alloy A2 (x=27); (c) Alloy A3 (x=35); (d) Alloy A4 (x=41); (e) Alloy A5 (x=49); (f) Alloy A6 (x=55); (g) Alloy A7 (x=60); (h) Alloy A8 (x=66)

that Alloys A1−A5 are composed of a single FCC solid solution. Different relative intensities of the XRD characteristic peaks indicate different orientations of the FCC phase. As can be seen from Fig. 2(a), there are two regions of different contrasts in Alloy A1 ($Al_7Cr_{20}Fe_{13}Ni_{60}$). According to the EDS results in Table 1, they have similar chemical composition and the Al content in the darker area is slightly higher (1.7 at.%). The XRD pattern in Fig. 1(a) proves that both regions are composed of FCC phase. Just like the $Al_7Cr_{20}Fe_{20}Ni_{53}$ alloy in Ref. [22], Alloy A1 solidifies with an isomorphous reaction, and the later solidified phase has a slightly higher Al content and shows a net-like appearance. The same phenomenon also exists in Alloy A2 ($Al_7Cr_{20}Fe_{27}Ni_{46}$), as shown in Fig. 2(b), although the alloy has a higher Fe content. When the Fe content is up to 35−41 at.% (Alloys A3 and A4), an uniform FCC phase is observed. This means that the temperature region for the FCC + liquid phase region is very narrow for these alloys and the solidification rate after arc-melting is quick enough to prevent the composition segregation. Therefore, almost no composition difference is detected in any region.

When the Fe content is increased to 55 at.% (Alloy A6), the dark and net-like BCC phase is

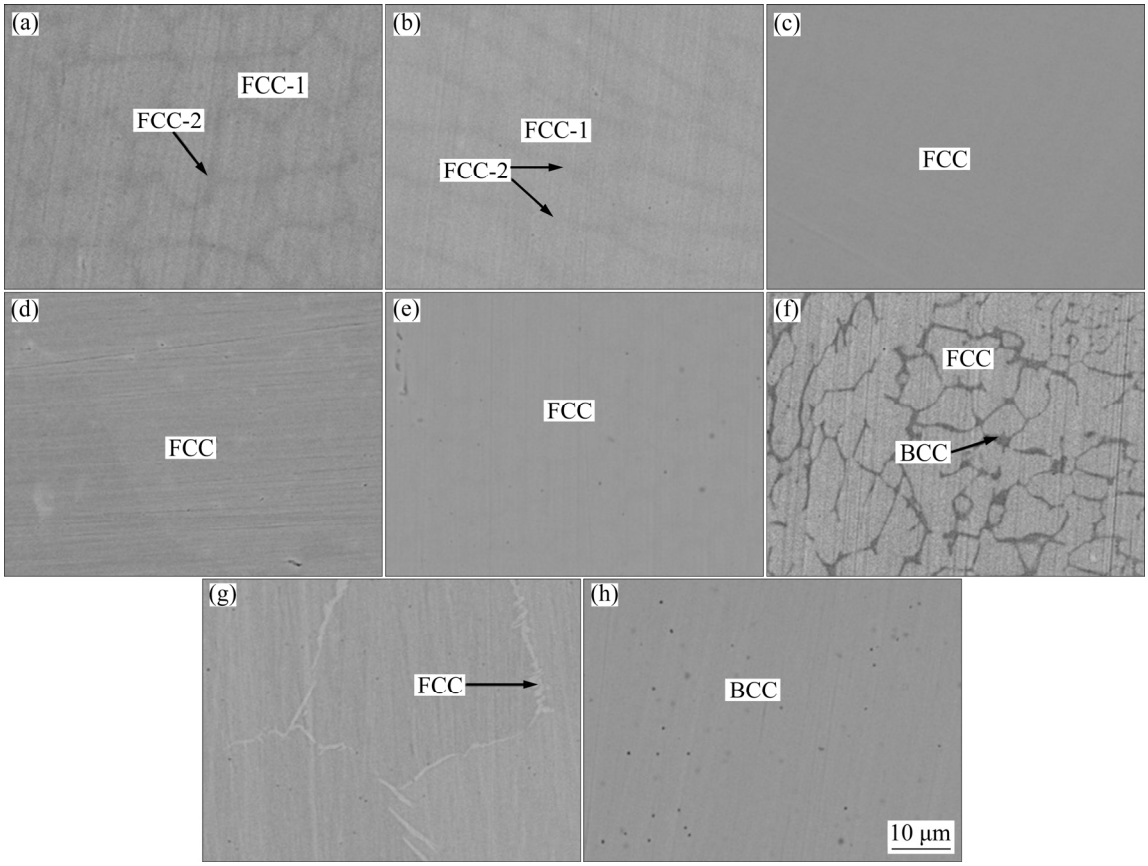

Fig. 2 BSE images of as-cast $Al_7Cr_{20}Fe_xNi_{73-x}$ alloys: (a) Alloy A1 (x=13); (b) Alloy A2 (x=27); (c) Alloy A3 (x=35); (d) Alloy A4 (x=41); (e) Alloy A5 (x=49); (f) Alloy A6 (x=55); (g) Alloy A7 (x=60); (h) Alloy A8 (x=66)

Table 1 Chemical compositions of different phases by EDS in as-cast $Al_7Cr_{20}Fe_xNi_{73-x}$ alloys

Designed composition	Alloy	Phase	Detected composition/at.%			
			Al	Cr	Fe	Ni
7Al−20Cr−13Fe−60Ni	A1	FCC-1	5.9	19.4	13.7	61.0
		FCC-2	7.6	21.0	12.6	58.8
7Al−20Cr−27Fe−46Ni	A2	FCC-1	6.0	19.9	27.8	46.3
		FCC-2	7.7	20.8	25.4	46.1
7Al−20Cr−55Fe−18Ni	A6	BCC	7.1	20.9	54.4	17.6
		FCC	6.1	20.2	55.2	18.5
7Al−20Cr−60Fe−13Ni	A7	FCC	5.4	19.6	61.0	14.0
		BCC	6.2	20.6	60.1	13.1
7Al−20Cr−66Fe−7Ni	A8	BCC	7.0	20.3	65.4	7.3

obvious in FCC matrix, as shown in Fig. 2(f). A weak BCC characteristic peak can be observed in the XRD pattern of Alloy A6 (Fig. 1(f)). EDS results in Table 1 show that the Al content in the as-cast BCC phase is just 1.0 at.% higher than that in the FCC phase. Some tiny dark spots are also observed in Alloy A5 ($Al_7Cr_{20}Fe_{49}Ni_{24}$). They are too small to be clearly detected, but they should be the BCC phase, as deduced from the phase constituent in Alloy A6.

With the increase of Fe content, the major phase in Alloy A7 ($Al_7Cr_{20}Fe_{60}Ni_{13}$) turns to be BCC, and no FCC phase is detected in Alloy A8 ($Al_7Cr_{20}Fe_{66}Ni_7$). A small amount of tiny black *B*2 spots can be observed in the BSE image (Fig. 2(h)). It should be pointed out that the BCC phase has a similar composition to the FCC phase, and the Fe-rich alloys always undergo the FCC to BCC transformation during cooling. To confirm this transformation, Alloy A8 was examined by DSC with a heating rate of 10 °C/min. The DSC curve shown in Fig. 3 indicates that there is a phase transformation at around 900 °C, which is near the allotropic transformation of Fe.

3.2 1000 °C-annealed $Al_7Cr_{20}Fe_xNi_{73-x}$ alloys

After annealing at 1000 °C for 30 d, the FCC phase in Alloys A'1 and A'2 becomes uniform, as shown in Figs. 4(a, b). In Alloys A'3−A'5 (Figs. 4(c, e)), a small amount of black BCC-type phase is precipitated from the FCC matrix after annealing. A small peak at ~45° (2θ) can be

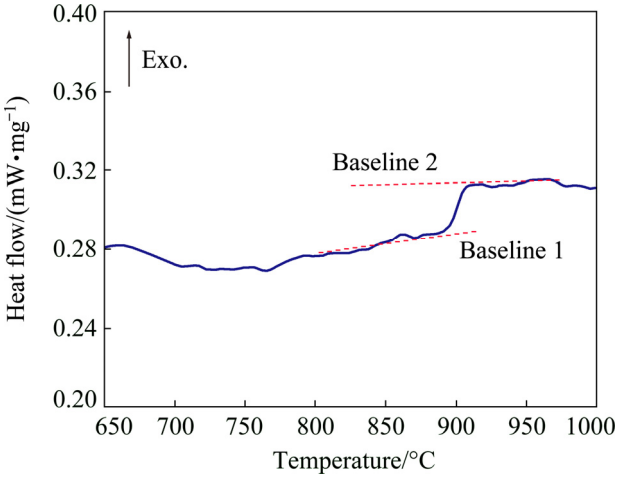

Fig. 3 DSC curve of Alloy A8 ($Al_7Cr_{20}Fe_{66}Ni_7$) with heating rate of 10 °C/min

observed in these alloys. This corresponds to the BCC-type phase, as shown in the XRD pattern of Alloy A′4 in Fig. 5. As pointed out by SUN et al [2], the ordered *B*2 phase can be distinguished from the BCC solid solution based on its XRD pattern and chemical composition. As listed in Table 2, the black phase has a very high Al content (≥27.0 at.%) and low Cr content (≤6.4 at.%). Therefore, the darker blocks should be the *B*2 phase. As for the Alloy A'6, the net-like BCC phase in the as-cast state turns into the Al-rich *B*2 phase after annealing at 1000 °C for 30 d. Its BSE image in Fig. 4(e) is similar to that of Alloy A'5. When the Fe content is above 60 at.%, in Alloys A'7 and A'8, the major phase in these alloys is the BCC phase; while no FCC phase is detected in the quenched alloy and some black *B*2 phase can be observed, as shown in Figs. 4(f, g). The EDS results in Table 2 indicate that the *B*2 phase contains 33.4 at.% Al and 42.2 at.% Ni, which is similar to that in Alloys A'4−A'6. As seen from Fig. 4(h), the grain size of the dot-like *B*2 phase decreases markedly. Similar to as-cast alloys, the FCC to BCC transformation should occur during cooling.

3.3 800 °C-annealed $Al_7Cr_{20}Fe_xNi_{73-x}$ alloys

After being annealed at 800 °C for 30 d, the microstructures of the $Al_7Cr_{20}Fe_xNi_{73-x}$ alloys change obviously. Their XRD patterns and BSE images are shown in Figs. 6 and 7, respectively. Also, only the BCC-type and/or FCC-type phases exist in these alloys. Compared to the 1000 °C-annealed alloys, the precipitates are much smaller

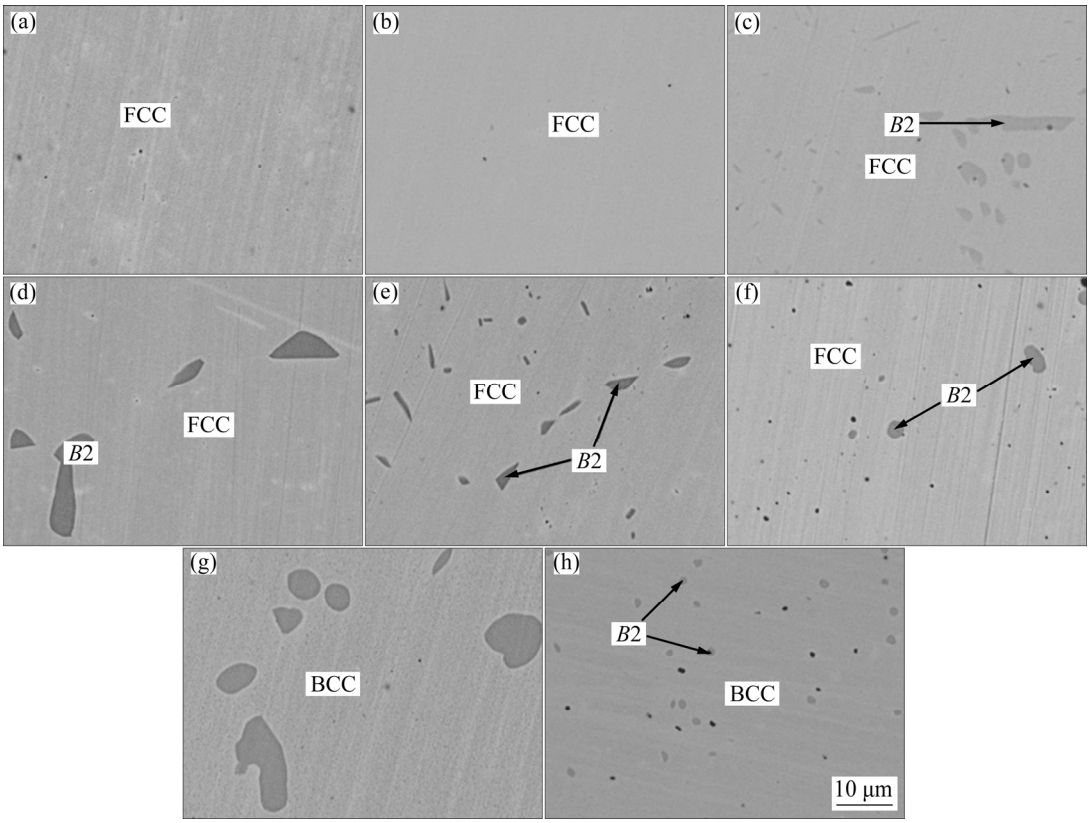

Fig. 4 BSE images of $Al_7Cr_{20}Fe_xNi_{73-x}$ alloys annealed at 1000 °C for 30 d: (a) Alloy A'1 (x=13); (b) Alloy A'2 (x=27); (c) Alloy A'3 (x=35); (d) Alloy A'4 (x=41); (e) Alloy A'5 (x=49); (f) Alloy A'6 (x=55); (g) Alloy A'7 (x=60); (h) Alloy A'8 (x=66)

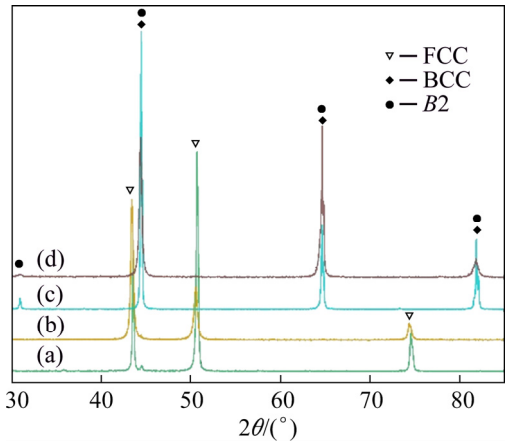

Fig. 5 XRD patterns of $Al_7Cr_{20}Fe_xNi_{73-x}$ annealed at 1000 °C for 30 d: (a) Alloy A'4 (x=41); (b) Alloy A'6 (x=55); (c) Alloy A'7 (x=60); (d) Alloy A'8 (x=66)

and the Al content in the FCC phase becomes much lower, as shown in Table 3.

As can be seen in Fig. 7(b), some black precipitates can be observed in the BSE image of Alloy A"2. These are identified as *B*2 phase for the same reason as presented above. Almost no darker precipitates can be observed in the phase boundary

Table 2 Chemical compositions of different phases in $Al_7Cr_{20}Fe_xNi_{73-x}$ alloys annealed at 1000 °C for 30 d

Designed composition	Alloy	Phase	Detected composition/at.%			
			Al	Cr	Fe	Ni
7Al−20Cr−35Fe−38Ni	A'3	FCC	6.3	20.8	34.2	38.7
		*B*2	31.5	4.5	12.4	51.6
7Al−20Cr−41Fe−32Ni	A'4	FCC	6.1	19.5	41.2	33.2
		*B*2	27.0	6.4	18.0	48.6
7Al−20Cr−49Fe−24Ni	A'5	FCC	6.0	20.0	49.2	24.8
		*B*2	31.0	5.7	18.3	45.0
7Al−20Cr−55Fe−18Ni	A'6	FCC	6.0	20.6	54.9	18.5
		*B*2	30.8	6.0	20.2	43.0
7Al−20Cr−60Fe−13Ni	A'7	BCC	7.8	20.9	60.9	10.4
		*B*2	33.4	3.9	20.5	42.2
7Al−20Cr−66Fe−7Ni	A'8	BCC	6.5	20.0	66.1	7.4
		*B*2	35.4	3.1	18.6	42.9

of Alloy A"1 after 800 °C annealing (Fig. 7(a)). Compared with the as-cast alloys, the *B*2 phase in the 800 °C-annealed alloys has a higher Al content,

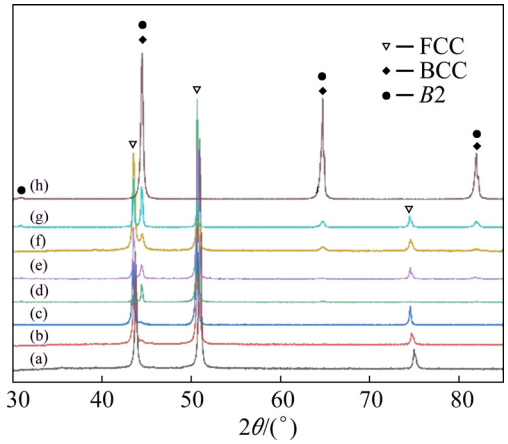

Fig. 6 XRD patterns of $Al_7Cr_{20}Fe_xNi_{73-x}$ alloys annealed at 800 °C for 30 d: (a) Alloy A"1 (x=13); (b) Alloy A"2 (x=27); (c) Alloy A"3 (x=35); (d) Alloy A"4 (x=41); (e) Alloy A"5 (x=49); (f) Alloy A"6 (x=55); (g) Alloy A"7 (x=60); (h) Alloy A"8 (x=66)

as shown in Table 3. With the increase of the Fe content, more *B*2 phase precipitates at the grain boundaries of Alloys A"3−A"5. Moreover, a small amount of BCC phase with less than 10 at.% Al and a little brighter color is precipitated in both the FCC matrix and at the phase boundaries. As can be seen from the BSE images of Alloys A"4 and A"5 in Figs. 7(d, e), the volume fraction of the BCC phase increases with the Fe content. The characteristic BCC peaks can be observed in their respective XRD patterns, as presented in Fig. 6.

For a fuller investigation of the precipitates in the FCC phase after 800 °C annealing, Alloy A"5 was examined by TEM. The image and the corresponding selected area electron diffraction (SAED) pattern are shown in Fig. 8. It can be seen that rod-like BCC nanocrystallites randomly distribute in the FCC matrix. Most particles have a width of less than 100 nm, even the alloy is annealed at 800 °C for 30 d. As can be seen from Fig. 7(e), the precipitates are homogeneously distributed in the FCC matrix, which will help to strengthen the alloys.

The grain size of the BCC and *B*2 phases becomes much larger when the Fe content is above 55 at.%. The dot-like *B*2 phase is uniformly distributed in these alloys. As can be seen in the

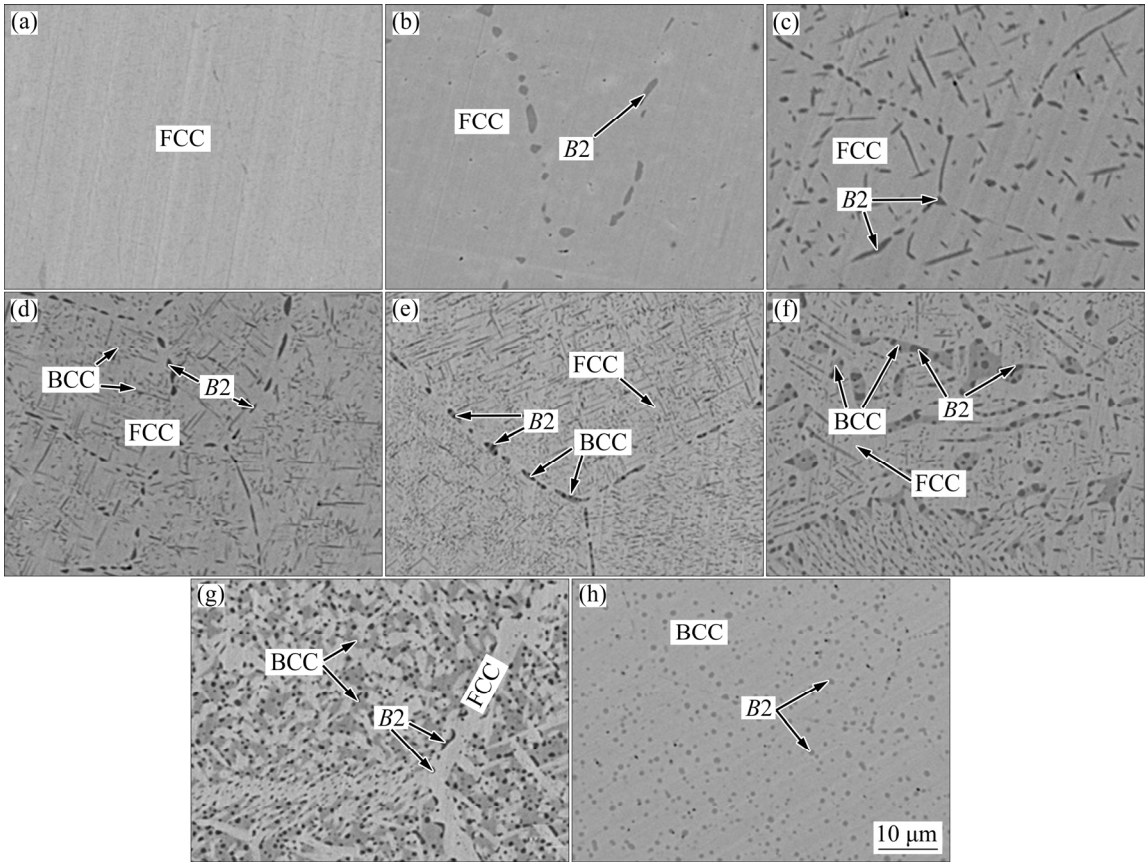

Fig. 7 BSE images of $Al_7Cr_{20}Fe_xNi_{73-x}$ alloys annealed at 800 °C for 30 d: (a) Alloy A"1 (x=13); (b) Alloy A"2 (x=27); (c) Alloy A"3 (x=35); (d) Alloy A"4 (x=41); (e) Alloy A"5 (x=49); (f) Alloy A"6 (x=55); (g) Alloy A"7 (x=60); (h) Alloy A"8 (x=66)

Table 3 Chemical compositions of different phases in $Al_7Cr_{20}Fe_xNi_{73-x}$ alloys annealed at 800 °C for 30 d

Designed composition	Alloy	Phase	Detected composition/at.%			
			Al	Cr	Fe	Ni
7Al−20Cr−27Fe−46Ni	A"2	FCC	5.4	19.8	27.2	47.6
		*B*2	28.3	4.1	9.7	57.9
7Al−20Cr−35Fe−38Ni	A"3	FCC	5.0	21.0	36.4	37.6
		*B*2	17.9	12.5	23.3	46.3
7Al−20Cr−41Fe−32Ni	A"4	FCC	4.0	21.4	43.4	31.2
		BCC	9.3	19.1	38.9	32.7
		*B*2	27.3	6.1	16.4	50.2
7Al−20Cr−49Fe−24Ni	A"5	FCC	4.3	21.2	51.6	22.9
		BCC	5.2	36.5	43.2	15.1
		*B*2	22.7	13.9	25.0	38.4
7Al−20Cr−55Fe−18Ni	A"6	FCC	3.1	19.9	60.4	16.6
		BCC	6.0	28.7	50.3	15.0
		*B*2	21.4	17.1	31.1	30.4
7Al−20Cr−60Fe−13Ni	A"7	FCC	5.0	17.7	63.3	14.0
		BCC	3.4	27.4	63.0	6.2
		*B*2	22.8	14.0	34.0	29.2
7Al−20Cr−66Fe−7Ni	A"8	BCC	5.8	20.6	68.0	5.6
		*B*2	15.2	16.4	53.5	14.9

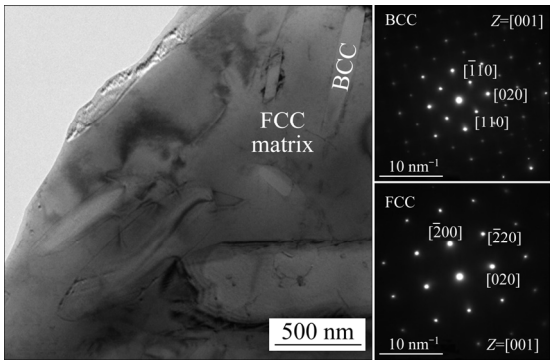

Fig. 8 TEM image and corresponding selected area electron diffraction patterns of $Al_7Cr_{20}Fe_{49}Ni_{24}$ (A"5) alloy annealed at 800 °C for 30 d

XRD pattern (Fig. 6(f)) and BSE image (Fig. 7(f)) of Alloy A"7, the large dendritic-like FCC phase is stable after annealing at 800 °C. The volume fraction of the BCC phase in Alloy A"7 is around 40 at.%, and its Al and Ni content decreases while its Fe content is 2.6% higher than that of Alloy A8. The fine dark *B*2 phase is distributed at the boundaries of the FCC and BCC phases. The BSE image of Alloy A"8 is similar to that of Alloy A′8, as can be seen from Figs. 7(g) and 5(g). The volume fraction of the dot-like *B*2 phase increases after 800 °C annealing.

After annealing at 1000 °C for 30 d, the alloys reach the equilibrium. As can be seen from Tables 1−3, the composition of the precipitated *B*2 phase is 27.0−35.4 at.% Al, 3.1−6.4 at.% Cr, 18.0−20.5 at.% Fe and 42.2−51.6 at.% Ni. This varies a little with the Fe and Ni contents. Although the *B*2 phase exists in both the Al−Fe and Al−Ni binary systems, the *B*2 phase in the Al−Cr−Fe−Ni quaternary system is a Ni-rich one.

3.4 Microhardness

Figure 9 shows the microhardness of the $Al_7Cr_{20}Fe_xNi_{73-x}$ alloys in three kinds of states. It is obvious that, when the Fe content is below 41 at.%, the hardness decreases a little with the increase of Fe content. Annealing at 1000 °C for 30 d has no significant effect on the hardness of these alloys, although a small amount of *B*2 phase precipitates. The hardness of the alloys even decreases with 50−55 at.% Fe. This is because the precipitation of the *B*2 phase decreases the Al content in the FCC phase and softens the FCC phase. When the Fe content is above 41 at.%, the hardness of the as-cast alloys increases with the Fe content due to the formation of the BCC-type phase. However, annealing at 1000 °C for 30 d softens these alloys, which is also caused by the decreasing Al content in the FCC matrix.

As can be seen from Fig. 9, annealing at 800 °C for 30 d can harden the alloys when the Fe content is 35−55 at.%. This is due to precipitation of the BCC phase in the FCC matrix, as discussed

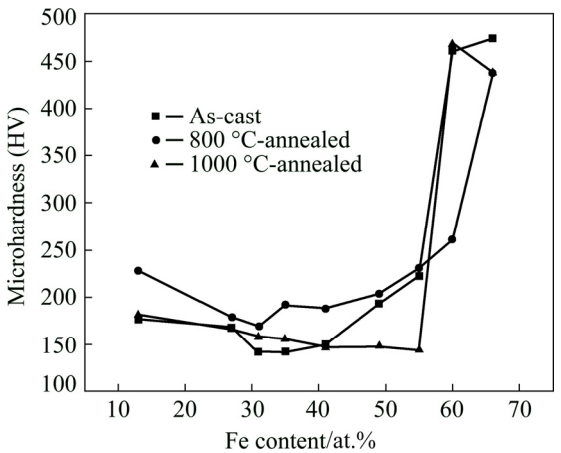

Fig. 9 Microhardness of as-cast or annealed $Al_7Cr_{20}Fe_xNi_{73-x}$ alloys

above. However, the microhardness of Alloy A"7 ($Al_7Cr_{20}Fe_{60}Ni_{13}$) markedly decreases after 800 °C annealing, for the existence of the stable FCC phase. As presented above, the BCC phase in Alloy A7 or Alloy A′7 is transformed from FCC phase during cooling. As for Alloy A"8, the BCC and *B*2 phases are stable at this temperature and the BCC phase can tolerate a lower Al content. It is worthy to note that, although the alloys can be dramatically hardened by the transformation of FCC to BCC during cooling, this also leads to high internal stress [33] and worsens the mechanical properties of the alloy.

It is well known that the alloys with FCC-type structure have better plastic formability than those with BCC-type structure. As discussed above, three types of phases exist in the $Al_7Cr_{20}Fe_xNi_{73-x}$ alloys. Most of these as-cast alloys are composed of the FCC phase. That is to say, hot-rolling is possible at higher temperatures. For the precipitation of the BCC or *B*2 phase after annealing, these alloys can be strengthened by aging, for example at 800 °C. Of course, a higher Al content leads to higher hardness. LIU et al [23] reported that, after homogenization, hot-rolling, and annealing at 1000 °C, the $Al_8Cr_{33.5}$-$Fe_{25}Ni_{33.5}$ alloy displayed an excellent combination of strength (yield strength is ~635 MPa and fracture strength is ~1155 MPa) and ductility (tension strain is ~11%). The results also show that the alloy strength is dramatically affected by the Al content. As can be seen from the chemical composition in Tables 1−3 and the published data, the FCC phase can tolerate less than 7 at.% Al. There is a large composition range that varies with the Fe and Ni content. The solubility of Al in the FCC phase decreases with decreasing the annealing temperature.

4 Conclusions

(1) Not all the as-cast $Al_7Cr_{20}Fe_xNi_{73-x}$ alloys are composed of single FCC phase. The FCC to BCC transformation at near 900 °C during cooling results in the existence of the BCC phase in the as-cast Fe-rich $Al_7Cr_{20}Fe_xNi_{73-x}$ alloys.

(2) After annealing at 1000 °C for 30 d, the Al content in the FCC solid solution decreases and the microhardness of the alloys decreases. A small amount of Al-rich *B*2 particles precipitate at the phase boundary and some rod-like BCC nanocrystallites precipitating in the FCC matrix increase the hardness of the 800 °C-annealed $Al_7Cr_{20}Fe_xNi_{73-x}$ (x=41−49) alloys.

(3) The FCC phase is stable in the 800 °C-annealed $Al_7Cr_{20}Fe_{60}Ni_{13}$ alloy, which decreases the hardness of the alloy.

(4) The *B*2 phase has a large composition range of 27.0−35.4 at.% Al, 3.1−6.4 at.% Cr, 18.0−20.5 at.% Fe and 42.2−51.6 at.% Ni. It has a higher Ni content and can only tolerate less than 6.4 at.% Cr.

Acknowledgments

The authors are grateful for the financial supports from the National Natural Science Foundation of China (51771035, 51671037), Natural Science Foundation of Jiangsu Province, China (BK20161190), and the Priority Academic Program of Jiangsu Higher Education Institutions, China.

References

[1] ZHANG Yong, ZUO Ting-ting, TANG Zhi, GAO M C, DAHMEN K A, LIAW P K, LU Zhao-ping. Microstructures and properties of high-entropy alloys [J]. Progress in Materials Science, 2014, 61: 1−93.

[2] SUN Ya, WU Chang-jun, PENG Hao-ping, LIU Ya, WANG Jian-hua, SU Xu-ping. Phase constituent and microhardness of as-cast and long-time annealed $Al_xCo_{2-x}CrFeNi$ multicomponent alloys [J]. Journal of Phase Equilibria and Diffusion, 2019, 40 (5): 706−714.

[3] WANG Y P, LI B S, REN M X, YANG C, FU H Z. Microstructure and compressive properties of AlCrFeCoNi high entropy alloy [J]. Materials Science and Engineering A, 2008, 491: 154−158.

[4] DONG Yong, ZHOU Kai-yao, LU Yi-ping, GAO Xiao-xia, WANG Tong-min, LI Ting-ju. Effect of vanadium addition on the microstructure and properties of AlCoCrFeNi high entropy alloy [J]. Materials & Design, 2014, 57: 67−72.

[5] WANI I S, BHATTACHARJEE T, SHEIKH S, BHATTACHARJEE P P, GUO S, TSUJI N. Tailoring nanostructures and mechanical properties of $AlCoCrFeNi_{2.1}$ eutectic high entropy alloy using thermo-mechanical processing [J]. Materials Science and Engineering A, 2016, 675: 99−109.

[6] ZHOU Shang-cheng, ZHANG Peng, XUE Yun-fei, WANG Fu-chi, WANG Lu, CAO Tang-qing, TAN Zhen, CHENG Bao-yuan, WANG Ben-peng. Microstructure evolution of $Al_{0.6}CoCrFeNi$ high entropy alloy powder prepared by high

pressure gas atomization [J]. Transactions of Nonferrous Metals Society of China, 2018, 28(5): 939−945.

[7] DONG Yong, LU Yi-ping, KONG Jiao-run, ZHANG Jun-jia, LI Ting-ju. Microstructure and mechanical properties of multi-component $AlCrFeNiMo_x$ high-entropy alloys [J]. Journal of Alloys and Compounds, 2013, 573: 96−101.

[8] JIANG Li, JIANG Hui, LU Yi-ping, WANG Tong-min, CAO Zhi-qiang, LI Ting-ju. Mechanical properties improvement of $AlCrFeNi_2Ti_{0.5}$ high entropy alloy through annealing design and its relationship with its particle-reinforced microstructures [J]. Journal of Materials Science & Technology, 2015, 31(4): 397−402.

[9] MUNITZ A, MESHI L, KAUFMAN M J. Heat treatments' effects on the microstructure and mechanical properties of an equiatomic Al−Cr−Fe−Mn−Ni high entropy alloy [J]. Materials Science and Engineering A, 2017, 689: 384−394.

[10] TONG Chung-Jin, CHEN Min-Rui, YEH Jien-Wei, LIN Su-Jien, CHEN Swe-Kai, SHUN Tao-Tsung, CHANG Shou-Yi. Mechanical performance of the $Al_xCoCrCuFeNi$ high-entropy alloy system with multiprincipal elements [J]. Metallurgical and Materials Transactions A, 2005, 36: 1263−1271.

[11] WU Jien-Min, LIN Su-Jien, YEH Jien-Wei, CHEN Swe-Kai, HUANG Yuan-Sheng, CHEN Hung-Cheng. Adhesive wear behavior of $Al_xCoCrCuFeNi$ high-entropy alloys as a function of aluminum content [J]. Wear, 2006, 261(5): 513−519.

[12] HEMPHILL M A, YUAN T, WANG G Y, YEH J W, TSAI C W, CHUANG A, LIAW P K. Fatigue behavior of $Al_{0.5}CoCrCuFeNi$ high entropy alloys [J]. Acta Materialia, 2012, 60(16): 5723−5734.

[13] IVCHENKO M V, PUSHIN V G, UKSUSNIKOV A N, WANDERKA N. Microstructure features of high-entropy equiatomic cast AlCrFeCoNiCu alloys [J]. The Physics of Metals and Metallography, 2013, 114(6): 514−520.

[14] MANZONI A, DAOUD H, MONDAL S, van SMAALEN S, VÖLKL R, GLATZEL U, WANDERKA N. Investigation of phases in $Al_{23}Co_{15}Cr_{23}Cu_8Fe_{15}Ni_{16}$ and $Al_8Co_{17}Cr_{17}Cu_8Fe_{17}Ni_{33}$ high entropy alloys and comparison with equilibrium phases predicted by Thermo-Calc [J]. Journal of Alloys and Compounds, 2013, 552: 430−436.

[15] XU Jun, CAO Cheng-ming, GU Ping, PENG Liang-ming. Microstructures, tensile properties and serrated flow of $Al_xCrMnFeCoNi$ high entropy alloys [J]. Transactions of Nonferrous Metals Society of China, 2020, 30(3): 746−755.

[16] HSU Chin-You, SHEU Tsing-Shien, YEH Jien-Wei, CHEN Swe-Kai. Effect of iron content on wear behavior of $AlCoCrFe_xMo_{0.5}Ni$ high-entropy alloys [J]. Wear, 2010, 268(5−6): 653−659.

[17] ZHU J M, ZHANG H F, FU H M, WANG A M, LI H, HU Z Q. Microstructures and compressive properties of multicomponent $AlCoCrCuFeNiMo_x$ alloys [J]. Journal of Alloys and Compounds, 2010, 497(1−2): 52−56.

[18] JUAN Chien-Chang, HSU Chin-You, TSAI Che-Wei, WANG Woei-Ren, SHEU Tsing-Shien, YEH Jien-Wei, CHEN Swe-Kai. On microstructure and mechanical performance of $AlCoCrFeMo_{0.5}Ni_x$ high-entropy alloys [J]. Intermetallics, 2013, 32: 401−407.

[19] WANG Zhi-jun, GUO Sheng, LIU C T. Phase selection in high-entropy alloys: From nonequilibrium to equilibrium [J]. JOM, 2014, 66(10): 1966−1972.

[20] SUN Ya, WU Chang-jun, LIU Ya, PENG Hao-ping, SU Xu-ping. Impact of alloying elements on the phase composition and mechanical properties of the CoCrFeNi-based high entropy alloys: A review [J]. Materials Reports, 2019, 33(4): 1169−1173. (in Chinese)

[21] CHEN Gan, WANG Lu, YANG Jin, LI Qian, LYU Pin, MA Sheng-guo. Mechanical properties and deformation mechanisms of $Al_{0.1}CoCrFeNi$ high-entropy alloys [J]. Journal of Materials Engineering, 2019, 47(1): 106−111.

[22] ZENG Jiao-feng, WU Chang-jun, PENG Hao-ping, LIU Ya, WANG Jian-hua, SU Xu-ping. Microstructure and microhardness of as-cast and 800 °C annealed $Al_xCr_{0.2}Fe_{0.2}Ni_{0.6-x}$ and $Al_{0.2}Cr_{0.2}Fe_yNi_{0.6-y}$ alloys [J]. Vacuum, 2018, 152: 214−221.

[23] LIU Man, ZUO Lei, LI Xuan, LI Ran, ZHANG Tao. Microstructure and mechanical properties of $Al_{25-x}Cr_{25+0.5x}Fe_{25}Ni_{25+0.5x}$ (x=19, 17, 15 at%) multi-component alloys [J]. Advanced Engineering Materials, 2018, 20(7): 1701057.

[24] YU Wei-wei, QU Ying-dong, LI Cheng-ze, LI Zhe, ZHANG Yu-feng, GUO Yao-zu, YOU Jun-hua, SU Rui-ming. Phase selection and mechanical properties of $(Al_{21.7}Cr_{15.8}Fe_{28.6}Ni_{33.9})_x(Al_{9.4}Cr_{19.7}Fe_{41.4}Ni_{29.5})_{100-x}$ high entropy alloys [J]. Materials Science and Engineering A, 2019, 751: 154−159.

[25] JIANG Zhen-fei, CHEN Wei-ping, XIA Ze-bang, XIONG Wei, FU Zhi-qiang. Influence of synthesis method on microstructure and mechanical behavior of Co-free AlCrFeNi medium-entropy alloy [J]. Intermetallics, 2019, 108: 45−54.

[26] SUI Yan-wei, GAO Shuo, CHEN Xiao, QI Ji-qiu, YANG Fei, WEI Fu-xiang, HE Ye-zeng, MENG Qing-kun, SUN Zhi. Microstructures and electrothermal properties of $Al_xCrFeNi$ multi-component alloys [J]. Vacuum, 2017, 144: 80−85.

[27] CHEN X, QI J Q, SUI Y W, HE Y Z, WEI F X, MENG Q K, SUN Z. Effects of aluminum on microstructure and compressive properties of Al−Cr−Fe−Ni eutectic multi-component alloys [J]. Materials Science and Engineering A, 2017, 681: 25−31.

[28] DU Y Y, LU Y P, LI T J, WANG T M, ZHANG G L. Effect of aluminium content of $Al_xCrFe_{1.5}Ni_{0.5}$ multiprincipal alloys on microstructure and alloy hardness [J]. Materials Research Innovations, 2011, 15(2): 107−110.

[29] DONG Yong, GAO Xiao-xia, LU Yi-ping, WANG Tong-min, LI Ting-ju. A multi-component $AlCrFe_2Ni_2$ alloy with excellent mechanical properties [J]. Materials Letters, 2016, 169: 62−64.

[30] JIN Xi, BI Juan, ZHANG Lu, ZHOU Yang, DU Xing-yu, LIANG Yu-xin, LI Bang-sheng. A new $CrFeNi_2Al$ eutectic high entropy alloy system with excellent mechanical properties [J]. Journal of Alloys and Compounds, 2019, 770: 655−661.

[31] YAO Kun-da, LIU Liang, SHANG Jian, ZHAO Zuo-fu,

ZHANG Yue, QI Jin-gang, WANG Bing. Microstructure and mechanical properties of $Al_{0.8}CrFe_2Ni_x$ high entropy alloys [J]. Special Casting & Nonferrous Alloys, 2020, 40(8): 880−883. (in Chinese)

[32] JIANG Shu-ying, LIN Zhi-feng, XU Hong-ming. Microstructure and properties of as-cast and annealed $Al_{0.5}CoCrFeNiTi_{0.5}$ high-entropy alloys [J]. The Chinese Journal of Nonferrous Metals, 2019, 29(2): 326−333. (in Chinese)

[33] BASU I, OCELíK V, de HOSSON J. BCC−FCC interfacial effects on plasticity and strengthening mechanisms in high entropy alloys [J]. Acta Materialia, 2018, 157: 83−95.

800 和 1000 °C 退火对 $Al_7Cr_{20}Fe_xNi_{73-x}$ 合金相析出和硬度的影响

吴长军[1,2]，周 琛[1]，曾姣凤[1]，刘 亚[1,2]，涂 浩[1,2]，苏旭平[1,2]

1. 常州大学 材料科学与工程学院 材料表面科学与技术江苏省重点实验室，常州 213164；
2. 常州大学 江苏省光伏科学与工程协同创新中心，常州 213164

摘 要：研究 Fe 含量对铸态、800 °C 和 1000 °C 退火后 $Al_7Cr_{20}Fe_xNi_{73-x}$ (x=13~66)合金的显微组织、相组成和显微硬度的影响。这些合金并非都由 FCC 单相组成，一些合金中存在 BCC 和 $B2$ 相。研究证实，$Al_7Cr_{20}Fe_{66}Ni_7$ 合金中的 BCC 相是在冷却过程中由 FCC 相在 900 °C 左右转变而来；而 FCC 相在 800 °C 退火后的 $Al_7Cr_{20}Fe_{60}Ni_{13}$ 合金中能稳定存在，从而导致富铁合金 800 °C 退火后硬度降低。实验结果表明，由于 $B2$ 粒子的析出，1000 °C 退火后的 FCC 相中 Al 含量降低，合金硬度降低。此外，800 °C 退火后，在晶界析出少量富 Al 的 $B2$ 颗粒及在 FCC 基体中析出一些纳米晶 BCC 相，使 $Al_7Cr_{20}Fe_xNi_{73-x}$ (x=41~49)合金硬度增加。这些结果将有助于 Al−Cr−Fe−Ni 基高熵合金的成分设计和加工工艺设计。

关键词：高熵合金；Al−Cr−Fe−Ni；相组成；显微硬度；热处理

(Edited by Bing YANG)